Materials Science and Engineering B 267 (2021) 115109

Contents lists available at ScienceDirect

Materials Science & Engineering B

journal homepage: www.elsevier.com/locate/mseb

Broad band photoluminescence of g-C_3N_4/ZnO/ZnS composite towards white light source

E.B. Chubenko [a,*], A.V. Baglov [a], M.S. Leanenia [b], B.D. Urmanov [b], V.E. Borisenko [a,c]

[a] Belarusian State University of Informatics and Radioelectronics, 220013 P.Brovka str. 6, Minsk, Belarus
[b] B. I. Stepanov Institute of Physics of the National Academy of Sciences of Belarus, 220072 Nezavisimosti ave., 68-2, Minsk, Belarus
[c] National Research Nuclear University MEPhI, 115409 Kashirskoe hwy, 31, Moscow, Russia

ARTICLE INFO

Keywords:
Graphitic carbon nitride
Zinc oxide
Zinc sulfide
Photoluminescence
Scanning electron microscopy
Composite

ABSTRACT

We have found one step synthesized g–C_3N_4/ZnO/ZnS composite to be promising for engineering of white-light sources. The composite was fabricated by simultaneous pyrolytic decomposition of thiourea and zinc acetate with a consequent *in situ* polymerization of the products at 550–625 °C and characterized by SEM, XRD, EDX and low temperature PL spectroscopy. The composite synthesized at 550 °C demonstrates blue PL with a peak at 2.74 eV while higher temperatures of the synthesis result in a broad spectra with a maximum at 2.22 eV and comprise of the bands of g–C_3N_4 and mixed ZnO/ZnS as they have been resolved by low temperature PL. The proper selection of the synthesis temperature allows an extension of light emitting spectra of g–C_3N_4/ZnO/ZnS composites from blue to white light range. The results obtained show ternary systems containing g-C_3N_4 and wide band-gap semiconductors are suitable for white-light emitting and optoelectronic devices.

1. Introduction

In the last decades, graphitic carbon nitride (g-C_3N_4) became a subject of an intensive study in the field of photocatalysis due to the good combination of its basic properties: high chemical and temperature stability, broad absorption spectra, large specific area and a lot of surface states participating in photocatalytic reactions [1-5]. Such interest has a reason. Nowadays modern society faces a lot of ecological challenges concerning water contamination with industrial and urban wastes and air pollutions from burning hydrocarbon fuels and industrial emissions. Some of them can be overwhelmed by utilization of photocatalytical systems using "green" solar energy [6–9]. Photocatalytic coatings can be also used to evaluate hydrogen from water under the sun light [7,10-12].

Outstanding photocatalytic properties of g-C_3N_4 leave in a shadow its attractive luminescent characteristics. Native blue temperature dependant tunable luminescence of this material [13,14] can be in principle combined with luminescence of other materials to cover a white-light range [15,16]. Despite the fact that many composites consisting of g-C_3N_4 and other semiconductors including binary and ternary systems were investigated [3-5] they were rarely considered for light–emitting purposes.

To obtain heterojunction system with broad emission spectra in the visible range g-C_3N_4 can be combined with chalcogenide semiconductors such as zinc oxide (ZnO) or zinc sulfide (ZnS) which are known for their high luminescence efficiency defined by the direct band gap structure [3]. ZnO is an important semiconductor material with many promising applications in optoelectronics, photovoltaics, sensors and photocatalythic systems [17-20]. Wide band gap of 3.37 eV at room temperature and high exciton binding energy (60 meV) of ZnO [17] provide good optoelectronic and photocatalytic characteristics in the ultraviolet spectral range [21,22]. However, strong intrinsic electron conductance and weak absorption in the visible range prove that coupling of ZnO with other semiconductor materials is needed to improve its characteristics [21,23]. ZnS is another wide band gap (up to 3.60 eV at room temperature) material possessing higher reduction potential than ZnO [7,22]. g-C_3N_4/ZnO/ZnS composites fabricated by multi step technological routs [7,24,25] were already indicated as a good photocatalysts but their luminescent properties were not well studied yet, especially at low temperatures. However combination of blue-green g–C_3N_4 luminescence with yellow–red ZnO/ZnS defect bands provides opportunity to use g–C_3N_4/ZnO/ZnS composites as phosphorus to fabricate white or colored light sources based on ultraviolet or blue LEDs. That phosphorus-on-LED approach is already proved to be

* Corresponding author.
E-mail address: eugene.chubenko@gmail.com (E.B. Chubenko).

https://doi.org/10.1016/j.mseb.2021.115109
Received 2 July 2020; Received in revised form 25 January 2021; Accepted 15 February 2021
Available online 1 March 2021

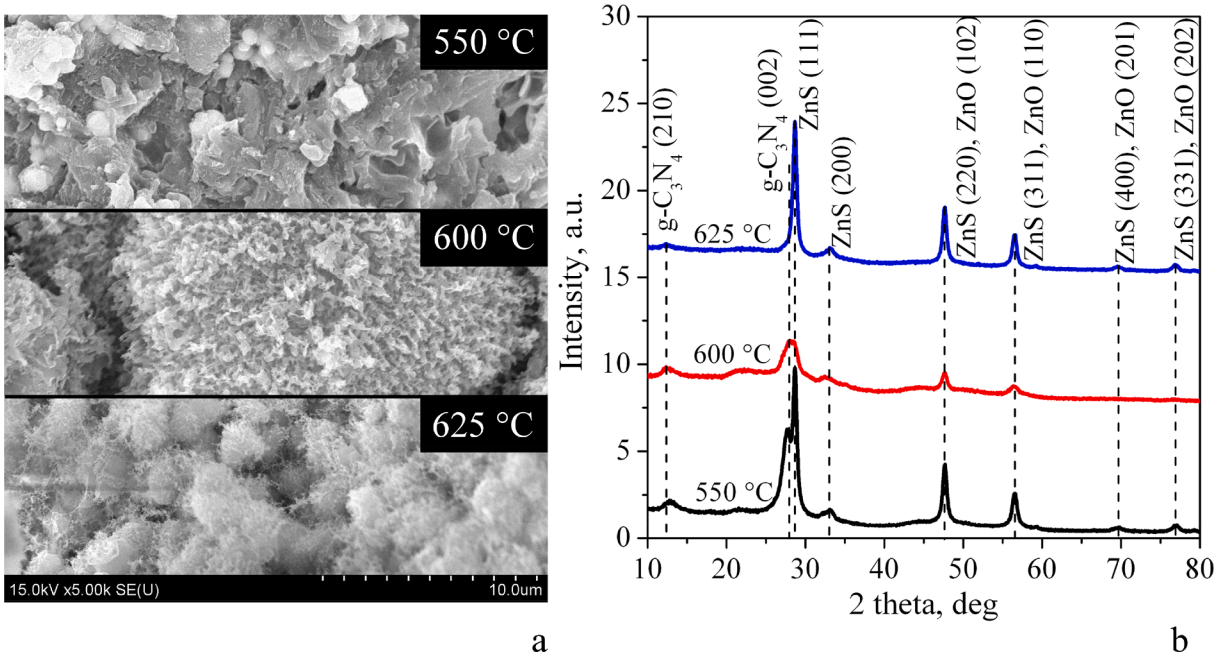

Fig. 1. SEM images of the surface (a) and XRD plot (b) of the materials synthesized at different temperatures from the mixture of thiourea and zinc acetate dehydrate.

conventional for the semiconductor white-light emitting devices [26]. Also electrical pumping of g–C_3N_4/ZnO/ZnS can not be excluded.

Our experiments presented in this paper were focused on the detailed study of photoluminescence (PL) in the wide temperature range from 10 to 300 K of g–C_3N_4/ZnO/ZnS heterojunction composites synthesized by novel simplified one-step pyrolytic process involving simultaneous decomposition of thiourea and zinc acetate with an idea to find out a way for engineering of white-light sources.

2. Materials and methods

Composites g-C_3N_4/ZnO/ZnS were synthesized within one step process by thermal decomposition of thiourea and zinc acetate dehydrate and subsequent *in situ* polymerization of the products in the oxygen containing ambient at 550–625 °C in the manner described before [14,27,28]. The precursors of an analytical grade at an equal amount by mass were placed inside ceramic crucible which was sealed with an aluminum gasket. Sealing prevented diffusion of ambient air from outside of the crucible but did not block evaporation and escaping of gaseous species from it. The crucible was placed inside a muffle furnace

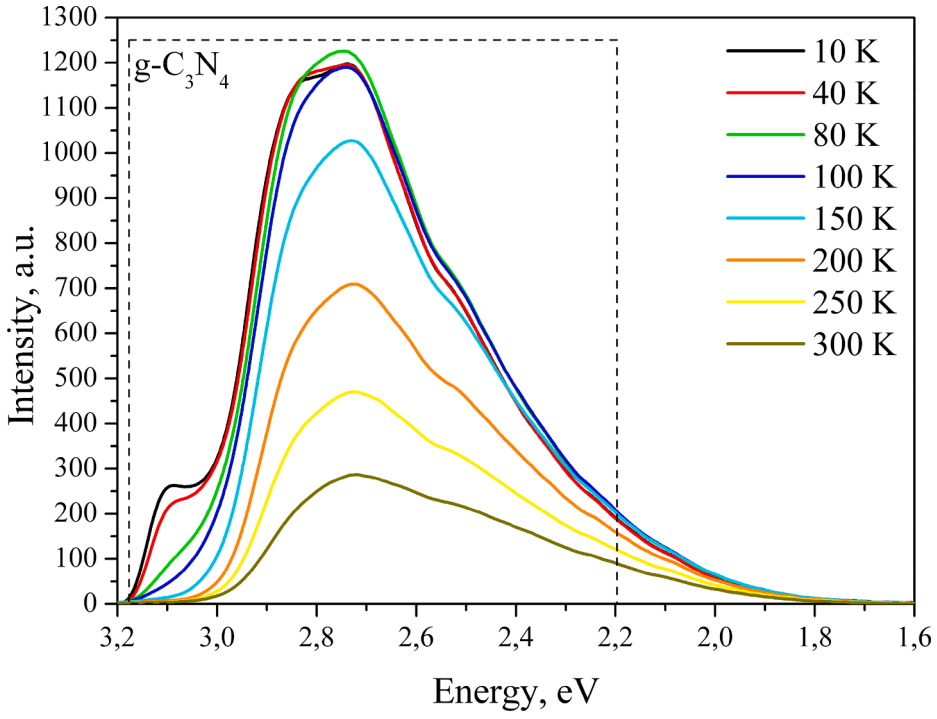

Fig. 2. PL spectra of the g-C_3N_4/ZnO/ZnS composite synthesized at 550 °C measured in the temperature range 10–300 K.

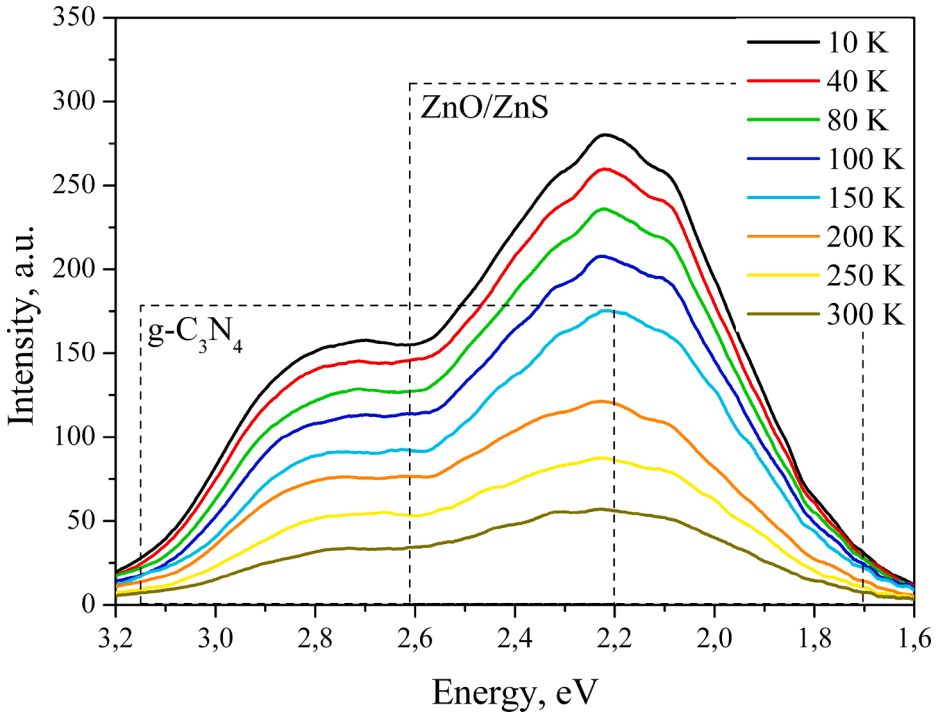

Fig. 3. PL spectra of the g-C_3N_4/ZnO/ZnS composite synthesized at 600 °C measured in the temperature range 10–300 K.

and heated to a target temperature at the rate of about 5 °C/min, kept for 30 min and cooled down to room temperature for 12 h.

The morphology of the synthesized g-C_3N_4/ZnO/ZnS composites was studied with Hitachi S–4800 scanning electron microscope (SEM). Their atomic composition was analyzed by energy-dispersive X-ray spectroscopy (EDX) using Bruker QUANTAX 200 EDX spectrometer. Crystalline phases in the composites were identified by X-ray diffraction analysis (XRD) using DRON-4 diffractometer (λ = 1.54184 Å).

Photoluminescence (PL) spectra were recorded in the temperature range of 10–300 K using closed cycle helium cryostat under excitation by HeCd-laser radiation (λ = 325 nm) with optical power density of about 0.1 W/cm^2. Solar LS SDH-VI spectrometer was used for registration of the PL spectra.

3. Results

The as-synthesized samples had a form of porous monolithic ingot dark yellow–brown in color. They were milled down in an agate mortar

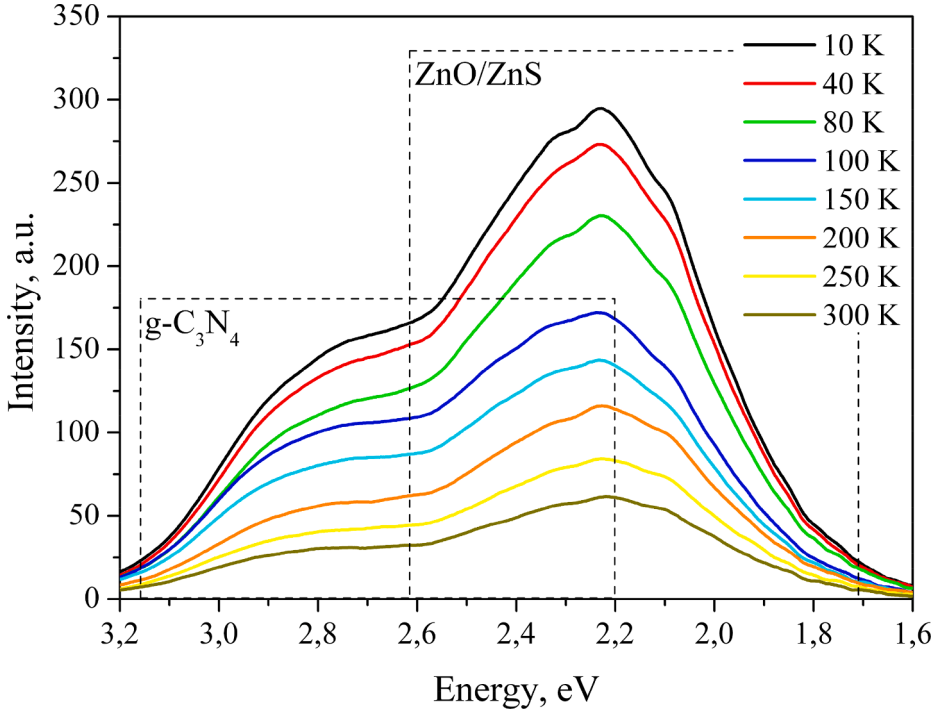

Fig. 4. PL spectra of the g-C_3N_4/ZnO/ZnS composite synthesized at 625 °C measured in the temperature range 10–300 K.

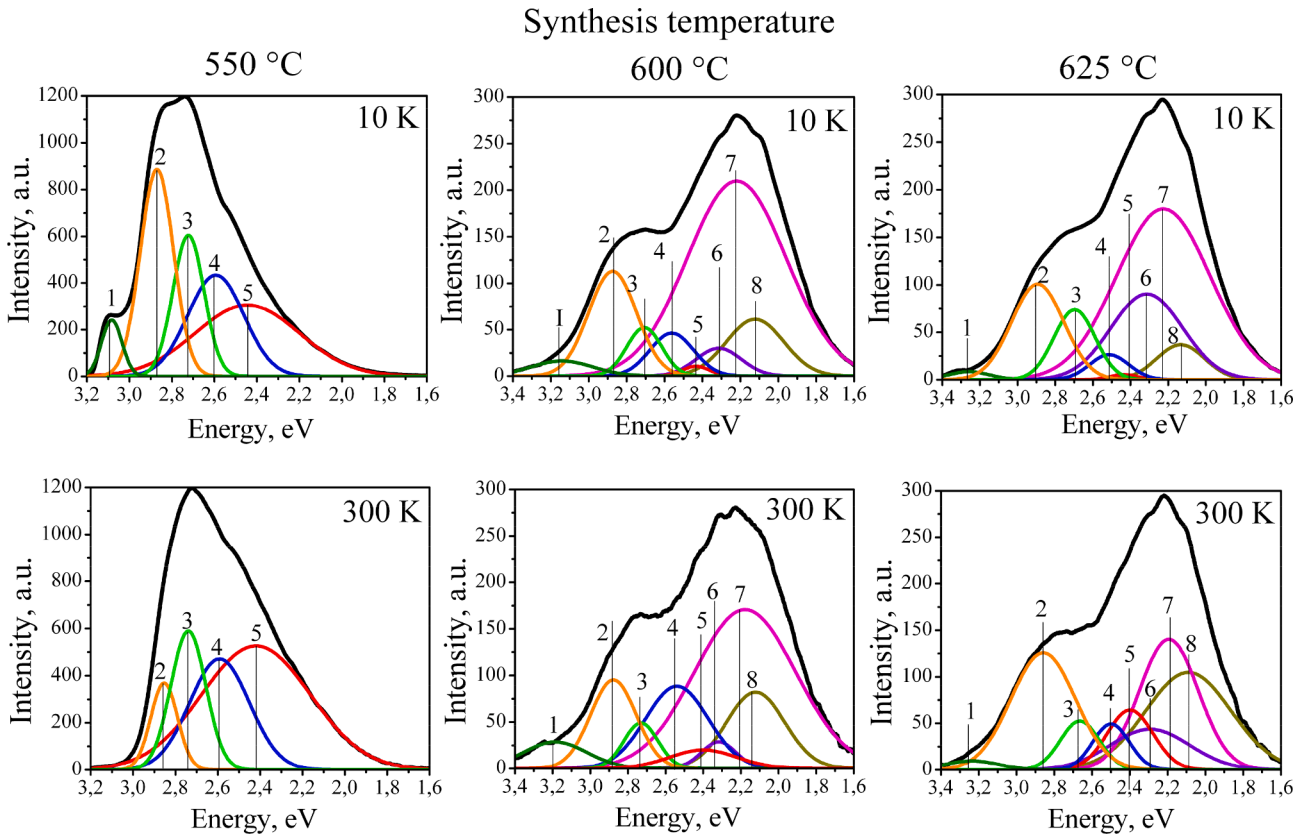

Fig. 5. Fitting with Gauss functions of the 10 K and 300 K PL spectra of the composites synthesized at different temperatures.

before the subsequent analysis. SEM images showed that the synthesized material consisted of compact crystals covered with flake-like species. With an increase of the synthesis temperature up to 625 °C the flakes became more and more perforated and begun to extinct (Fig. 1, a). Availing for the performed XRD analysis compact crystals may be identified as ZnO and ZnS semiconductor particles. The flakes can be referred to g-C_3N_4 because it is known that this organic polymer begin to decompose at temperatures higher than 600 °C [1,3,29] that is why the perforations occur.

EDX analysis showed that oxygen concentration appeared to be not higher than in g–C_3N_4 synthesized at the same conditions and temperature from thiourea [14] and do not exceed 7.45–8.4 at.%. The C/N atomic concentration ratio varies from 0.81 at 550 °C to 0.84 at 625 °C. That numbers is higher than the stoichiometric value for g-C_3N_4 equal to 0.75. During the synthesis it is not possible to overwhelm the kinetic limit associated with evaporation of carbon in volatile species (HCN and C_2N_2) produced by partial decomposition of g-C_3N_4 at temperatures above 540 °C [30]. Thus, carbon in the synthesized material can be presented in the elementary form as a result of combustion of carbon containing residue from the acetic acid (CH_3COO^-) in a closed space. The Zn/S concentration ratio is mach higher than the stoichiometric value for crystalline ZnS (obviously equal to 1) across whole studied temperature range, and increases to 4.6 at synthesis temperature of 625 °C from 1.77 at 550 °C. Remaining zinc can be bonded to oxygen forming ZnO clusters.

The XRD analysis (Fig. 1, b) showed the presence of polymerized g-C_3N_4 in the composite. Two typical peaks located at $2\theta = 12.8$ deg and $2\theta = 27.5$ deg are presented on the XRD spectra of the samples synthesized at 550–625 °C. They associate with g-C_3N_4 (210) and (002) phases [29]. The XRD spectra also contain a number of peaks corresponding to crystalline ZnS with cubic sphalerite structure and ZnO with hexagonal wurtzite structure: at $2\theta = 33.2$ deg – ZnS (200), 47.6 deg – ZnS (220) and ZnO (102), 56.5 deg – ZnS (311) and ZnO (110), 69.5 deg – ZnS (400) and ZnO (201), 76.9 deg – ZnS (331) and ZnO (202). g-C_3N_4 (002) plane peak at 27.5 deg can also overlap with ZnS (111) plane peak at 28.6 deg and seem to disappear at synthesis temperature of 625 °C.

Table 1
Energy positions (in eV) of the peaks corresponding to the bands in the PL spectra of the g-C_3N_4/ZnO/ZnS composites synthesized at different temperatures (the band numbers correspond to those in Fig. 5).

Measurement temperature, K		10			300		
Synthesis temperature, °C		550	600	650	550	600	650
Band number	1	3.083	3.14	3.259	–	3.187	3.236
	2	2.87	2.874	2.893	2.853	2.877	2.859
	3	2.722	2.707	2.697	2.739	2.731	2.665
	4	2.593	2.562	2.513	2.592	2.54	2.5
	5	2.445	2.434	2.437	2.42	2.34	2.399
	6	–	2.314	2.313	–	2.318	2.293
	7	–	2.22	2.226	–	2.178	2.193
	8	–	2.122	2.133		2.122	2.09

Low and room temperature PL spectra of the g-C_3N_4/ZnO/ZnS composite synthesized at 550 °C measured in the temperature range 10–300 K are presented in Fig. 2. They are typical for unmodified g-C_3N_4 fabricated at the same temperature 550 °C [13,14,31]. The spectra of the composite have complex structure and include several overlapping bands corresponding to different transitions between energy bands in the g-C_3N_4. Maximum of the integral spectra is located at 2.74 eV. Its intensity gradually drops with an increase of the measurement temperature. Emission bands corresponding to the ZnS or ZnO band-to-band transitions were not found.

PL spectra of the g-C_3N_4/ZnO/ZnS composites synthesized at 600 and 625 °C also measured in the same temperature range from 10 to 300 K shown in Figs. 3 and 4 significantly differ from the ones of the sample fabricated at 550 °C. The most prominent is that new wide band with the

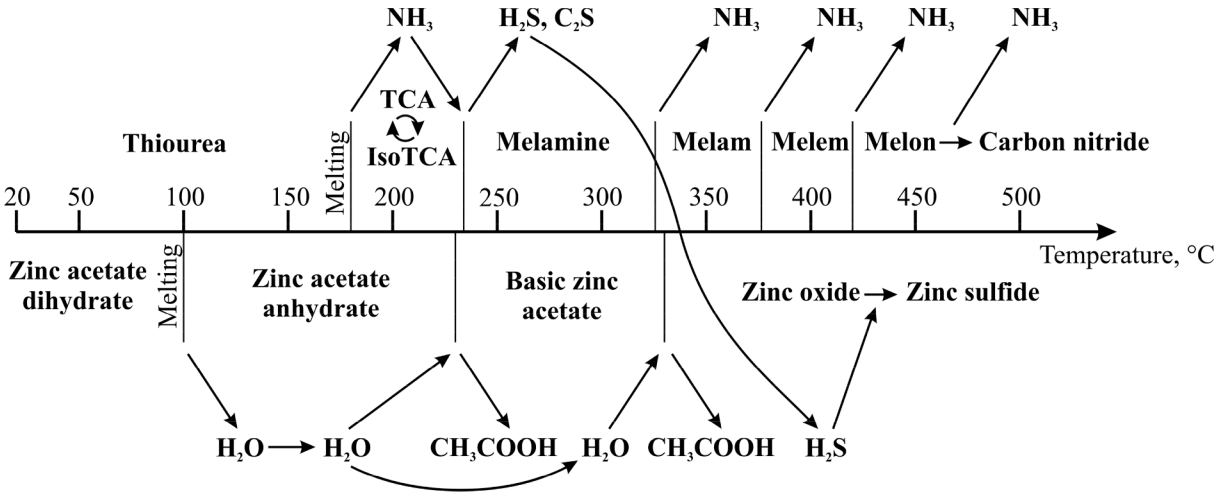

Fig. 6. Illustration of the g-C_3N_4/ZnO/ZnS composite synthesis process. Diagram built using data from references [36-42].

maximum located approximately at 2.22 eV has appeared. This extended band consists of few sub-bands.

Fitting of the PL spectra with Gauss functions reveals some common bands illustrated in Fig. 5 and summarized in Table 1. The bands from 1 to 5 can be identified as belonging to radiative transitions in g C_3N_4 [13,30,31]. The bands 6–8 correspond to radiative transitions in ZnS or ZnO [20,32-34] and are not resolved in the spectra of the sample synthesised at 550 °C.

Some specific features can be noted at the data presented in Table 1. First, the peak energy of each band decreases with an increase of the temperature. This phenomenon can be easily attributed to band-gap narrowing in semiconductors according to empirical Varshni equation [35]. Second, the intensity maximum of the g-C_3N_4 PL band shifts to lower energies with growing synthesis temperature.

4. Discussion

In our experiments two different precursors were mixed in a crucible and heated simultaneously. Each of them undergoes individual chemical transitions during thermal processing. Thiourea transforms to thiocyanic acid/isothiocyanic acid (TCA/IsoTCA) tautomers and then to melamine at approximately 230–240 °C losing ammonia [36] and sulphur containing gaseous species such as carbon disulfide (CS_2) and hydrogen sulphide (H_2S) [37]. That process is represented at the diagram on the Fig. 6. At an increasing temperature melamine consequently transforms to melam, melem, melon and then at 420 °C it begins to polymerize into g-C_3N_4 [29]. Due to the kinetic limit [30] polymerization of g-C_3N_4 is usually not completed leaving some of the melon polymeric chains not interconnected with each other.

Heated zinc acetate dyhydrate loses its water (H_2O) and acetic acid groups (CH_3COOH) and forms basic zinc acetate ($Zn_4O(CH_3COO)_6$) at approximately 235 °C [38-41]. At temperatures higher than 270 °C basic zinc acetate reacts with H_2O vapor resulting in a replacement of acetic acid groups with oxygen and formation of ZnO. That process is completed at 330 °C [38-40]. Formation of ZnS can be explained as a result of interaction of sulphur containing species (CS_2 and H_2S) in a closed volume of the ceramic crucible with ZnO synthesised from zinc acetate in the conditions of limited oxygen supply. The presence of ZnS

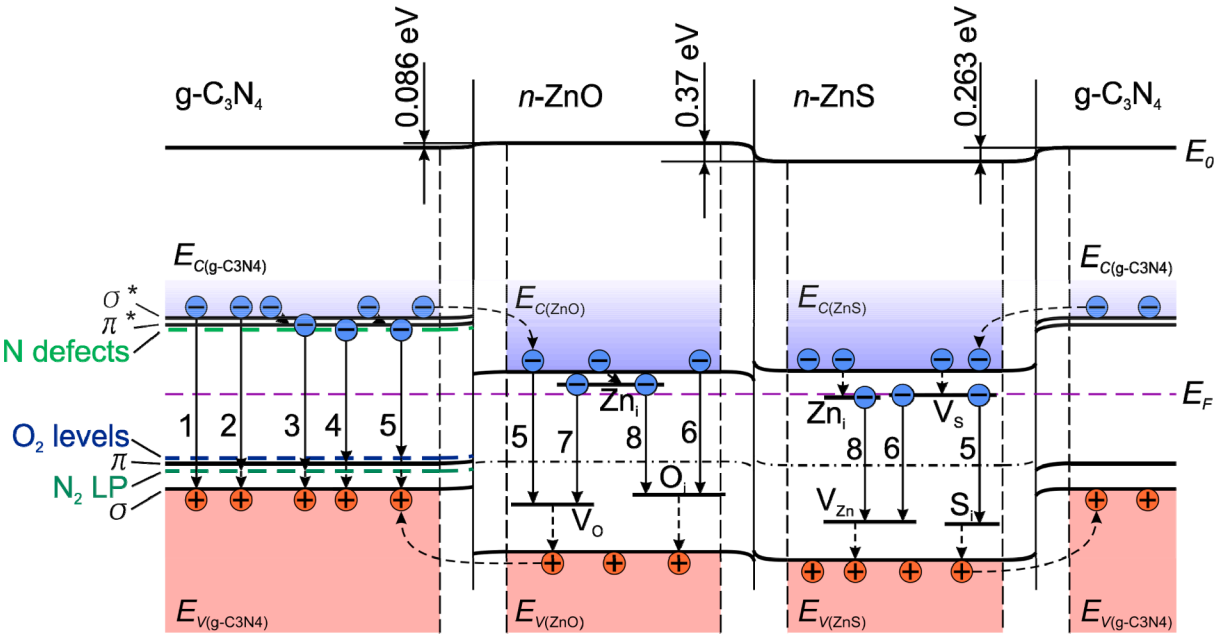

Fig. 7. Loop belt electron energy diagram of the g-C_3N_4/ZnO/ZnS heterojunction composite. Numbers indicate possible irradiative recombination routes and correspond to the numbers in Fig. 5. E_0 is the electron energy in vacuum.

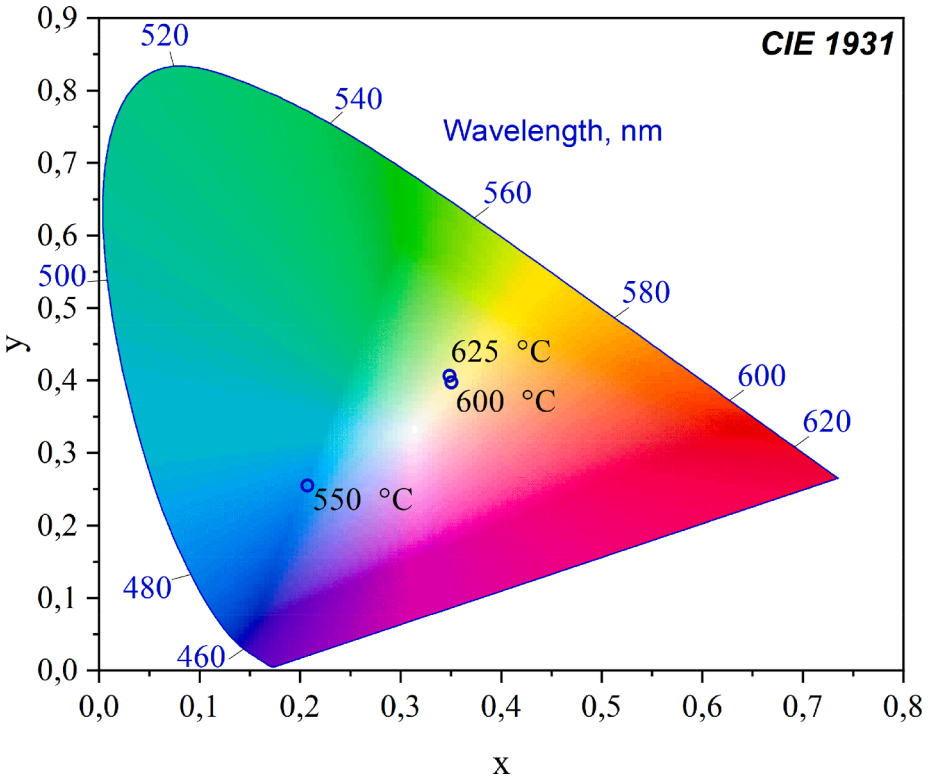

Fig. 8. CIE 1931 chromaticity diagram with the points representing the color of PL of g-C_3N_4/ZnO/ZnS heterojunction composite samples obtained at different temperatures (550–625 °C). PL spectra measured at 300 K were used to calculate position of the points.

is not usual because in the case of unlimited supply of oxygen it must oxidize to ZnO at temperatures above 300 °C [42]. It is also known, that ZnO is unstable in the acidic environment and easily reacts with acids (H_2S in that case) producing appropriated compounds (ZnS).

The condensation temperature of ZnO/ZnS (below 320 °C) is lower than that of g-C_3N_4 (higher than 420 °C). That is why g-C_3N_4 covers already formed ZnO/ZnS crystals. At the composite synthesis temperature of 550 °C PL of ZnO/ZnS is not visible because crystallites of these wide band gap semiconductors are screened with g-C_3N_4 flakes. Partial decomposition of g-C_3N_4 at higher temperatures leads to stripping of ZnO/ZnS and their PL begins to dominate in integral PL spectra.

In order to understand the PL spectra of the g-C_3N_4/ZnO/ZnS composite we constructed and analyzed its electron energy band structure presented in Fig. 7. There ZnO and ZnS are supposed to be *n*–type semiconductors accounting for intrinsic defects in these materials usually acting like donor impurities [19,33]. g-C_3N_4 is considered as an intrinsic semiconductor, *i.e.* the Fermi level E_F locates at around the energy band-gap center.

The registered PL spectra of g-C_3N_4 consist of five distinguishable bands corresponding to several recombination transition processes in its energy band structure. Its valence band ($E_{V(g\text{–}C3N4)}$) is formed by C-N σ-bonds with sp^3 hybridization and by π-bonds C-N with sp^2 hybridization as well as N_2 lone pairs (LP). Conduction band of g-C_3N_4 ($E_{C(g\text{-}C3N4)}$) is the superposition of excited σ- and π-bonds (marked correspondingly as σ^* and π^*) [43,44].

The bands composing the PL spectra of the material synthesized at 550 °C are defined by allowed radiative transitions between σ^* and σ energy levels (band 1 which becomes more prominent at lower measurement temperatures) [31], from σ^* to N_2 LP level (band 2) [43,44], π^*- N_2 LP transitions (band 3) [45,46], between nitrogen defects level (triple bonds C≡N, NH_2 groups and N vacancies) and N_2 LP (band 4) [43,47], transitions to oxygen defect energy levels (band 5) [43-45]. Blurring of bands 4 and 5 are supposed to be caused by energy dispersion of oxygen and nitrogen defect levels.

In the composites synthesized at 600 and 625 °C the band 5 also overlaps with possible transitions in ZnO and ZnS. These semiconductors usually have structural defects such as Zn vacancies and Zn interstitials as well as oxygen (or sulfur in the case of ZnS) vacancies and interstitials [17]. Excited electrons from the ZnO conduction band ($E_{C(ZnO)}$) can move to the oxygen vacancy levels (V_O) located near the valance band. The energy of $E_{C(ZnO)}$-V_O transition is 2.46 eV [47]. Approximately the same energy of 2.41 eV is typical for electron transitions in ZnS from the sulfur vacancy level V_S to the sulfur interstitial level S_i [35].

The energy of the band 6 corresponds to transitions from the $E_{C(ZnO)}$ in ZnO to oxygen interstitial levels (O_i). Its energy is 2.28 eV [47]. There is similar energy of 2.31 eV for transitions from sulfur vacancy level (V_S) in ZnS to zinc vacancy levels (V_{Zn}) [32]. An appearance of the band 7 is probably a result of radiative transitions of electrons from zinc interstitial atoms Zn_i in the ZnO band gap to V_O levels [47]. The energy of this transition is 2.24 eV. Transitions from zinc interstitial states (Zn_i) to O_i levels in ZnO (2.06 eV) as well as transitions from Zn_i to V_{Zn} in ZnS (2.00 eV) are considered to be responsible for the lowest energy band 8 [33,47].

A diffusion exchange of electrons and holes between the semiconductors in the heterojunction composite is supposed to influence the intensity of particular bands. In the contact regions conduction band electrons in g–C_3N_4 are energetically favored to move to ZnO and ZnS. As for holes, they can leave ZnO and ZnS moving to g–C_3N_4. Note that the balance in the charge carrier exchange can be controlled by an external electric bias which is useful for a design of light emitting devices.

PL spectra of g-C_3N_4/ZnO/ZnS heterojunction composite samples fabricated at different temperatures measured at 300 K were used to calculate chromaticity coordinates of the PL color. Obtained points were placed on the standard CIE 1931 chromaticity diagram (Fig. 8). According to presented diagram the color of the luminescence light form the sample synthesized at 550 °C can be considered as blue. The color of light irradiated by the samples synthesized at 600 and 625 °C is very

similar and matches to white domain [48].

5. Conclusion

Heterojunction g-C_3N_4/ZnO/ZnS composites synthesized by pyrolytic decomposition of thiourea and zinc acetate with a consequent *in situ* polymerization of the products in a closed ambient at 550–625 °C allow getting their room temperature luminescence varied from blue to white as a function of the synthesis temperature. Intrinsic defect states in the semiconductors are mainly involved in the radiative electron transitions. An appropriate choice of the synthesis conditions affords engineering of the spectrum of the emitted light. Moreover, a use of other precursors providing synthesis of g-C_3N_4 based heterojunction composites with other semiconducting oxides and chalcogenides can extend this opportunity. Such materials look promising for wide band visible light-emitting devices operating with optical or electrical pumping.

Declaration of Competing Interest

The authors declare that they have no known competing financial interests or personal relationships that could have appeared to influence the work reported in this paper.

Acknowledgements

This work was supported by the Belarus National Research Programs "Physical Materials Science, Novel Materials and Technologies" and "Photonics, Opto- and Microelectronics". The authors are grateful to D. V. Zhigulin for the SEM and EDX analysis of the samples, V. V. Uglov for XRD characterization of the samples, G. P. Yablonski for discussion of the results and fruitful comments. V. E. Borisenko acknowledges the partial financial support of the "Improving of the Competitiveness" Program of the National Research Nuclear University MEPhI – Moscow Engineering Physics Institute.

References

[1] J. Zhu, P. Xiao, H. Li, S.A.C. Carabineiro, ACS Appl. Mater. Interfaces 6 (2014) 16449–16465, https://doi.org/10.1021/am502925j.
[2] S. Yin, J. Han, T. Zhou, R. Xu, Catal. Sci. Technol. 5 (2015) 5048–5061, https://doi.org/10.1039/C5CY00938C.
[3] A. Sudhaik, P. Raizada, P. Shandilya, D.-Y. Jeong, J. Lim, P. Singh, J. Ind. Eng. Chem. 67 (2018) 28–51, https://doi.org/10.1016/j.jiec.2018.07.007.
[4] J. Wen, J. Xie, X. Chen, X. Li, Appl. Surf. Sci. 391 (2017) 72–123, https://doi.org/10.1016/j.apsusc.2016.07.030.
[5] M. Ismael, J. Alloys Compd. 846 (2020), 156446, https://doi.org/10.1016/j.jallcom.2020.156446.
[6] D. Spasiano, R. Marotta, S. Malato, P. Fernandez-Ibañez, I. Di Somma, Appl. Catal., B 170–171 (2015) 90–123, https://doi.org/10.1016/j.apcatb.2014.12.050.
[7] L. Yang, H. Zhou, T. Fan, D. Zhang, Phys. Chem. Chem. Phys. 16 (2014) 6810–6826, https://doi.org/10.1039/C4CP00246F.
[8] H. Zhou, Y. Qu, T. Zeid, X. Duan, Energy Environ. Sci. 5 (2012) 6732–6743, https://doi.org/10.1039/C2EE03447F.
[9] S. Thomas, D. Pasquini, S. Leu, D.A. Gopakumar (Eds.), Nanoscale Materials in Water Purification, Elsevier, Netherlands, 2019, pp. 581–651.
[10] A. Kudo, Y. Miseki, Chem. Soc. Rev. 38 (2009) 253–278, https://doi.org/10.1039/B800489G.
[11] M. Fellet, D.M. Tiede, MRS Bull. 42 (2017) 190–191, https://doi.org/10.1557/mrs.2017.35.
[12] L. Lin, T. Hisatomi, S. Chen, T. Takata, K. Domen, Trends Chem. 2 (2020) 813–824, https://doi.org/10.1016/j.trechm.2020.06.006.
[13] A.V. Baglov, E.B. Chubenko, A.A. Hnitsko, V.E. Borisenko, A.A. Malashevich, V. V. Uglov, Semicond. 54 (2020) 226–230, https://doi.org/10.1134/S1063782620020049.
[14] E.B. Chubenko, N.M. Denisov, A.V. Baglov, V.P. Bondarenko, V.V. Uglov, V. E. Borisenko, Cryst. Res. Technol. 55 (2020) 1900163, https://doi.org/10.1002/crat.201900163.
[15] Q. Guo, M. Wei, Z. Zheng, X. Huang, X. Song, S.-B. Qiu, X. Yang, X. Liu, J. Qiu, Adv. Optical Mater. 2019 (2019) 1900775, https://doi.org/10.1002/adom.201900775.
[16] B. Han, Y. Xue, P. Li, J. Zhang, J. Zhang, H. Shi, J. Solid State Chem. 232 (2015) 26–30, https://doi.org/10.1016/j.jssc.2015.08.046.
[17] Ü. Özgür, Y.I. Alivov, C. Liu, A. Teke, M.A. Reshchikov, S. Doğan, V. Avrutin, S.-J. Cho, H. Morkoç, Appl. Phys. Rev. 98 (2005), 041301, https://doi.org/10.1063/1.1992666.
[18] A. Kołodziejczak-Radzimska, T. Jesionowski, Materials 7 (2014) 2833–2881, https://doi.org/10.3390/ma7042833.
[19] Ü. Özgür, D. Hofstetter, H. Morko, Proc. IEEE 98 (2010) 1255–1268, https://doi.org/10.1109/JPROC.2010.2044550.
[20] A.B. Djurišić, X. Chen, Y.H. Leung, A.M.C. Ng, J. Mater. Chem. 22 (2012) 6526–6535, https://doi.org/10.1039/C2JM15548F.
[21] K.M. Lee, C.W. Lai, K.S. Ngai, J.C. Juan, Water Res. 88 (2016) 428–448, https://doi.org/10.1016/j.watres.2015.09.045.
[22] A. Hernández-Ramírez, I. Medina-Ramírez (Eds.), Photocatalytic Semiconductors: Synthesis, Characterization, and Environmental Applications, Springer International Publishing, Switzerland, 2015, pp. 1–9.
[23] S. Rehman, R. Ullah, A.M. Butt, N.D. Gohar, J. Hazard. Mater. 170 (2009) 560–569, https://doi.org/10.1016/j.jhazmat.2009.05.064.
[24] Z. Dong, Y. Wu, N. Thirugnanam, G. Li, Appl. Surf. Sci. 430 (2018) 293–300, https://doi.org/10.1016/j.apsusc.2017.07.186.
[25] C. Liu, Y. Qiu, F. Wang, K. Wang, Q. Liang, Z. Chen, Adv. Mater. Interfaces 4 (2017) 1700681, https://doi.org/10.1002/admi.201700681.
[26] J. Cho, J.H. Park, J.K. Kim, E.F. Schubert, Laser Photonics Rev. 11 (2017) 1600147, https://doi.org/10.1002/lpor.201600147.
[27] E.B. Chubenko, A.V. Baglov, E.S. Lisimova, V.E. Borisenko, Int. J. Nanosci. 18 (2019) 1940042, https://doi.org/10.1142/S0219581X19400428.
[28] N.M. Denisov, E.B. Chubenko, V.P. Bondarenko, V.E. Borisenko, Tech. Phys Lett. 45 (2019) 108–110, https://doi.org/10.1134/S1063785019020068.
[29] A. Thomas, A. Fischer, F. Goettmann, M. Antonietti, J.-O. Müller, R. Schlögl, J. M. Carlsson, Mater. Chem. 18 (2008) 4893–4908, https://doi.org/10.1039/B800274F.
[30] B. Jürgens, E. Irran, J. Senker, P. Kroll, H. Müller, W. Schnick, J. Am. Chem. Soc. 125 (2003) 10288–10300, https://doi.org/10.1021/ja0357689.
[31] E.B. Chubenko, A.V. Baglov, M.S. Leonenya, G.P. Yablonskii, V.E. Borisenko, J. Appl. Spectrosc. 87 (2020) 9–14, https://doi.org/10.1007/s10812-020-00954-y.
[32] J. Dong, X. Zeng, W. Xia, X. Zhang, M. Zhou, C. Wang, RSC Adv. 7 (2017) 20874–20881, https://doi.org/10.1039/C7RA02521A.
[33] X. Wang, J. Shi, Z. Feng, M. Li, C. Li, Phys. Chem. Chem. Phys. 13 (2011) 4715–4723, https://doi.org/10.1039/C0CP01620A.
[34] C.H. Ahn, Y.Y. Kim, D.C. Kim, S.K. Mohanta, H.K. Cho, J. Appl. Phys. 105 (2009), 013502, https://doi.org/10.1063/1.3054175.
[35] Y.P. Varshni, Physica 34 (1967) 149–154, https://doi.org/10.1016/0031-8914(67)90062-6.
[36] S.C. Moldoveanu, Pyrolysis of organic molecules. Applications to health and environmental issue, Elsevier Science, Amsterdam, 2019, pp. 697–714.
[37] G. Zhang, J. Zhang, M. Zhang, X. Wang, J. Mater. Chem. 22 (2012) 8083–8091, https://doi.org/10.1039/C2JM00097K.
[38] A.V. Ghule, B. Lo, S.-H. Tzing, K. Ghule, H. Chang, Y.C. Ling, Chem. Phys. Lett. 381 (2003) 262–270, https://doi.org/10.1016/j.cplett.2003.09.125.
[39] M. Singh, G. Palazzo, G. Romanazzi, G.P. Suranna, N. Ditaranto, C. Di Franco, M. V. Santacroce, M.Y. Mulla, M. Magliulo, K. Manolij, L. Torsi, Faraday Discuss. 174 (2014) 383–398, https://doi.org/10.1039/C4FD00081A.
[40] C.-C. Lin, Y.-Y. Li, Mater. Chem. Phys. 113 (2009) 334–337, https://doi.org/10.1016/j.matchemphys.2008.07.070.
[41] F. Paraguay, W. Estrada, D.R. Acosta, E. Andrade, M. Miki-Yoshida, Thin Solid Films 350 (1999) 192–202, https://doi.org/10.1016/S0040-6090(99)00050-4.
[42] R. Wahab, S.G. Ansari, Y.-S. Kim, M.S. Dhage, H.K. Seo, M. Song, H.-S. Shin, Met. Mater. Int. 15 (2009) 453–458, https://doi.org/10.1007/s12540-009-0453-5.
[43] B. Choudhury, K.K. Paul, D. Sanyal, A. Hazarika, P.K. Giri, J. Phys. Chem. C 122 (2018) 9209–9219, https://doi.org/10.1021/acs.jpcc.8b01388.
[44] Y. Jiang, Z. Sun, C. Tang, Y. Zhou, L. Zeng, L. Huang, Appl. Catal., B 240 (2019) 30–38, https://doi.org/10.1016/j.apcatb.2018.08.059.
[45] Y. Zhang, Q. Pan, G. Chai, M. Liang, G. Dong, Q. Zhang, J. Qiu, Sci. Rep. 3 (2013) 1943, https://doi.org/10.1038/srep01943.
[46] Z. Gan, Y. Shan, J. Chen, Q. Gui, Q. Zhang, S. Nie, X. Wu, Nano Res. 9 (2016) 1801–1812, https://doi.org/10.1007/s12274-016-1073-2.
[47] S. Vempati, J. Mitra, P. Dawson, Nanoscale Res. Lett. 7 (2012) 470, https://doi.org/10.1186/1556-276X-7-470.
[48] B. Fortner, T. Meyer, Number by Colors: A Guide to Using Color to Understand Technical Data, Springer, New York, 1997, pp. 87–118.